Chaotic bouncing of a droplet on a soap film

T. Gilet[1,*] and John W.M. Bush[2,†]

[1] *GRASP, Department of Physics B5a, University of Liège, B-4000 Liège, Belgium*

[2] *Department of Mathematics, Massachusetts Institute of Technology, Cambridge, MA 02139, USA*

We examine the complex dynamics arising when a water droplet bounces on a horizontal soap film suspended on a vertically oscillating circular frame. A variety of simple and complex periodic bouncing states are observed, in addition to multiperiodicity and period-doubling transitions to chaos. The system is simply and accurately modeled by a single ordinary differential equation, numerical solution of which captures all the essential features of the observed behaviour. Iterative maps and bifurcation diagrams indicate that the system exhibits all the features of a classic low-dimensional chaotic oscillator.

PACS numbers: 68.15.+e, 47.55.Dz, 68.03.Cd
Keywords: Droplet physics, Vibrated interface, Bouncing

Couder et al.[**?**] have recently shown that oil droplets, when placed on a vertically vibrated oil bath, may bounce indefinitely rather than coalescing. The dynamics of the bouncing droplets are extraordinarily rich. Feedback between the droplet and its wave field may lead to self-propulsion [**?**] and diffraction of these walking droplets as they pass through a slit [**?**]; moreover, multiple droplets may lock into complex orbital motions [**?**] or lattices [**?**]. We here demonstrate that a droplet on a vertically vibrated soap film may similarly avoid coalescence, and that the bouncing droplet represents a textbook example of a chaotic oscillator, with many features common to the bouncing of an inelastic ball on a solid substrate.

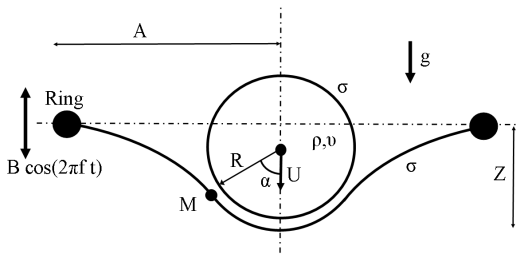

FIG. 1: Experimental system: a droplet of radius $R = 0.8$mm bounces on a soap film of radius $A = 16.0$mm vibrated with vertical displacement $B\cos\Omega t$. The soap film assumes the form of a spherical cap beneath the droplet, and a catenoid beyond the matching point M.

A droplet of radius $R = 0.08$cm bounces on an horizontal circular soap film of radius $A = 1.6$cm vibrated with vertical displacement $B\cos(2\pi ft)$ (Fig. **??**). The droplet and soap film consist of a glycerol-water-soap mixture (80% water, 20% glycerol, <1% soap) with density $\rho = 1.05$ g cm^{-3}, viscosity $\nu = 2$ cSt and surface tension $\sigma = 22$ dyn cm^{-1}. Drops of uniform size ($R = 0.8$ mm) and mass ($m = 2.25$ mg) were extruded from an insulin syringe (needle diameter 0.35 mm). For the bouncing states, the characteristic drop impact speeds ($U \sim 4 - 32$ cm s^{-1}) are much less than the characteristic wave speed on the film (a film thickness of 4 μm indicates a wave speed of $\sqrt{2\sigma/\rho h} \sim 330$ cm s^{-1}). The influence of capillary waves is thus assumed to be negligible, and the film described as quasistatic: it deforms instantaneously in response to the forcing imposed by the droplet. See EPAPS Document No.[ ] for a complete bouncing sequence. The Weber number $We = \rho U^2 R/\sigma$ lies between 0.06 and 3.9. During impact, the droplet remains roughly spherical: maximum centerline distortions of 13% were observed (at $We = 3.9$), so the surface energy of drop distortion is less than 3% that associated with soap film distortion. Beneath the droplet, the soap film lies tangent to the droplet, and so roughly assumes the form of a spherical cap of radius R. Beyond the droplet, the pressure is atmospheric on either side of the soap film, which thus assumes the form of a catenoid as confirmed experimentally. The spherical cap and catenoid match at a point M corresponding to an angle α (Fig.**??**). The vertical deflection of the soap film Z and the resulting vertical force F on the droplet may be expressed in terms of α:

$$\begin{aligned} \frac{Z}{R} &= 1 - \cos\alpha + \sin^2\alpha \ln\left[\frac{\tan\frac{\alpha}{2}}{\beta}\left(1+\sqrt{1-\beta^2}\right)\right] \\ F &= 4\pi\sigma R \sin^2\alpha \end{aligned} \qquad (1)$$

where $\beta = (R\sin^2\alpha)/A$. The force-displacement relation $F(Z)$ is shown in Fig.**??**(a). In the range $0 < Z/R < 3$, the film responds as a linear spring, $F = kZ$, where the effective spring constant $k = \frac{8\pi}{7}\sigma$. The force then saturates, achieving a maximum at $\alpha = \pi/2$, and decreases thereafter. This quasistatic description of the film was used successfully by the authors [**?**] to deduce a criterion for breakthrough of a droplet striking a stationary

*Electronic address: Tristan.Gilet@ulg.ac.be
†Electronic address: bush@math.mit.edu

film [**?**].

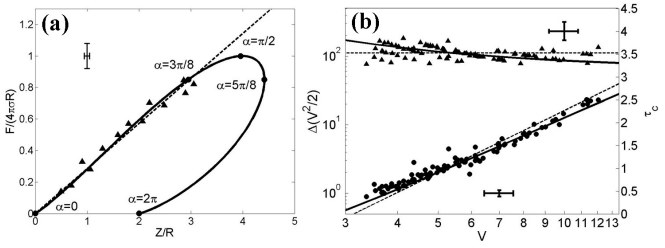

FIG. 2: (a) Relation between the maximum soap film deflection Z and the resulting vertical force F acting on the droplet. (▲) Experimental measurements inferred from droplet trajectories. The solid line corresponds to the theoretical approximation of the soap film shape (**??**). The dashed line is the linear approximation $F = 8\pi\sigma Z/7$, valid for $Z/R < 3$. (b) (Left axis - •) Energy dissipated, $\Delta(V^2/2)$, during impact on a static soap film as a function of the dimensionless impact speed $V = U/(g\tau_\sigma)$. The dashed line is the best-fit $\Delta(V^2/2) = 0.016V^3$. (Right axis - ▲) Contact time $\tau_c = t_c/\tau_\sigma$ as a function of the impact speed V. The dashed line is the best-fit law $\tau_c = 3.52$. The solid lines correspond to the numerical solution of Eq.(**??**) with $\Gamma = 0$ and $\Psi = 0.01$. Characteristic error bars are shown.

When the droplet strikes a static soap film at a speed U, the drop is in apparent contact with the film for a time t_c. Dissipation during rebound results in the kinetic energy at take-off being less than that at impact. Fig.**??**(b) illustrates the dependence of the dimensionless contact time $\tau_c = t_c/\tau_\sigma$ and dissipated energy $\Delta(V^2/2)$ on the dimensionless impact speed $V = U/(g\tau_\sigma)$, where $\tau_\sigma = \sqrt{m/k}$ and g is the gravitational acceleration. Note that the contact time is independent of the impact speed V and proportional to τ_c, as is consistent with the film behaving as a linear spring, and as was observed for droplets bouncing on hydrophobic substrates [**?**]. The dissipated energy increases as V^3, a scaling that we shall exploit in our theoretical modeling.

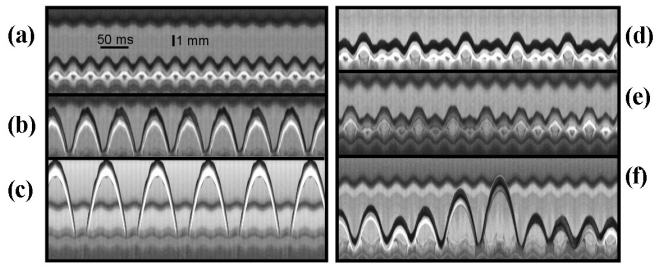

FIG. 3: Spatiotemporal diagrams of bouncing states observed experimentally at $\omega = 1.1$ ($f = 33$ Hz). The images are formed by compiling side by side vertical centerline columns of successive video images: time is represented by the horizontal coordinate. For a periodic bouncing state denoted by (m, n), the droplet bounces n times while the soap film oscillates m times. (a) Mode $(1, 1)$ at $\Gamma = 0.6$. (b) Mode $(2, 1)$ at $\Gamma = 0.6$. (c) Mode $(3, 1)$ at $\Gamma = 0.6$. (d) Mode $(3, 3)$ at $\Gamma = 0.7$. (e) Mode $(2, 2)$ at $\Gamma = 1.2$. (f) Chaotic motion at $\Gamma = 1.1$.

On a sinusoidally forced soap film, periodic bouncing occurs in the range where the soap film behaves as a linear spring (Fig.**??**). The droplet trajectory is prescribed by a force balance: the drop accelerates in response to gravity and the force applied by the soap film, the latter of which acts only when the drop is in apparent contact with the film. A dissipative force proportional to kU^2/g takes the dissipated energy, growing as V^3, into account. Writing the force balance in the accelerating reference frame of the bounding ring introduces a sinusoidal forcing term. In dimensionless form, the force balance thus assumes the form:

$$\frac{d^2y}{d\tau^2} = -H(-y)y - 1 - \Psi H(-y)|\dot{y}|\dot{y} + \Gamma\cos(\omega\tau + \phi) \ , \quad (2)$$

where $\tau = t/\tau_\sigma$, $y = -Z/(g\tau_\sigma^2)$, $\Gamma = 4\pi^2 Bf^2/g$, $\omega = 2\pi f\tau_\sigma$, and $H(y)$ is the Heaviside function. The coefficient $\Psi = 0.01$ is inferred from the experimental data reported in Fig.**??**(b). In many respects, numerical solution of Eq.(**??**) yields remarkably good agreement with the experimental data. In Fig.**??**(a), we demonstrate the excellent agreement between the observed trajectory of a drop released above an unforced film and that predicted by Eq.(**??**) for $\Gamma = 0$.

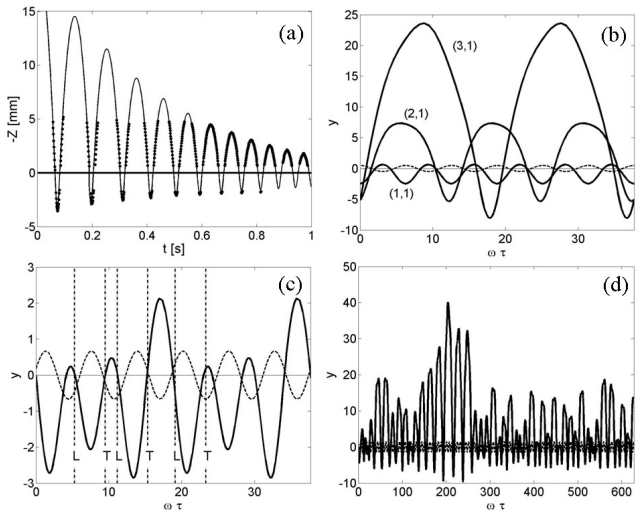

FIG. 4: Numerical solutions of Eq.(**??**) with a coefficient of dissipation $\Psi = 0.01$ inferred from Fig.**??**(b). (a) Observed (dots) and simulated (solid line) trajectories of a droplet bouncing on a stationary soap film ($\Gamma = 0$). (b) Modes $(1, 1), (2, 1)$ and $(3, 1)$ at $\Gamma = 0.6$. (c) Mode $(3, 3)$ at $\Gamma = 0.82$. The landing and take-off phases measured experimentally are represented by (L) and (T) vertical lines respectively. (d) Chaotic motion at $\Gamma = 2$. In (b - c), the dashed line indicates the ring motion.

The film forcing provides energy to the droplet. If this energy precisely balances that lost through dissipation during impact, the droplet executes a periodic bouncing motion. We denote by (m, n) a periodic state in which the droplet bounces n times and the soap film oscillates m

times during a single period. A myriad of simple ($n = 1$) and complex ($n > 1$) periodic states were observed experimentally, including $(1,1)$, $(2,1)$, $(3,1)$, $(3,3)$ and $(2,2)$ (Fig.**??**). Mode transitions characterized by either aperiodic transients or period doubling cascades were observed as the forcing parameters were varied (See EPAPS Document No.[ ]). Multiperiodicity is apparent in Fig.**??**(a-c): multiple periodic solutions $(1,1)$, $(2,1)$ and $(3,1)$ arise for precisely the same forcing parameters $(\omega, \Gamma) = (0.6, 1.1)$, but different initial conditions. With $\omega = 0.6$ fixed, complex periodic states were apparent at higher Γ (Fig.**??**d-e) and ultimately chaos emerges for $\Gamma \geq 1.1$ (Fig.**??**f). As seen in Fig.**??**(b-c), the computed periodic solutions of Eq.(**??**) are remarkably close to those observed experimentally; in particular, the landing and take-off phases are in good agreement. As a caveat, we note that complex modes $(m, n > 1)$ and the onset of chaotic motion are observed at slightly lower accelerations in the experiments than the numerics.

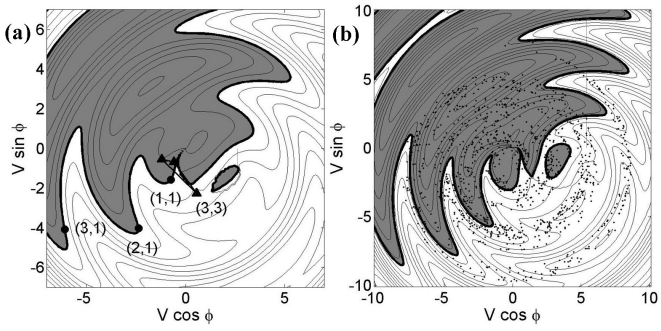

FIG. 5: Iterative maps (V, ϕ) in polar coordinates, with $(a$-$b)$ contours of energy transferred to the droplet, $V_{i+1}^2 - V_i^2$, as a function of the impact speed V and phase ϕ at $\omega = 1.1$. The droplet gains and loses energy when it impacts in, respectively, the shaded and white regions. (a) $\Gamma = 0.82$: $(\bullet)$ Simple periodic modes (m,1). $(\blacktriangle)$ Complex periodic mode (3,3). Contours are spaced by $\Delta(V^2) = 2$. (b) Chaotic solutions at $\Gamma = 1.82$. The dots correspond to the Poincaré section of a spiraling strange attractor. Contours are spaced by $\Delta(V^2) = 5$.

Solutions of Eq.(**??**) may be displayed on a Poincaré section by computing the speed and phase at impact, $(y, \dot{y}) = (0, -V)$. Equation (**??**) is integrated numerically from one impact to the next, for various initial conditions $(V,\ \phi)$. A two-dimensional iterative map may thus be defined as:

$$\begin{cases} V_{i+1} = f(V_i, \phi_i) \\ \phi_{i+1} = g(V_i, \phi_i)\ . \end{cases} \tag{3}$$

Poincaré sections are represented in Fig.**??**(a-b) for $\Gamma = 0.82$ and $\Gamma = 1.82$, respectively. For each set of initial conditions (V_i, ϕ_i), contours of the net energy acquired by the drop during impact, $V_{i+1}^2 - V_i^2$, are computed. The shaded area corresponds to initial conditions for which energy is gained during impact; in the white area, energy is lost. Simple modes $(m, 1)$ are represented by single points that necessarily lie on the boundary of the shaded area: no energy is gained or lost during impact, so the bouncing is perfectly periodic over a single forcing cycle. Complex modes $(m, n > 1)$ are represented by closed curves that cross the zero-energy boundary. For example, in the $(3,3)$ mode (Fig.**??**d and Fig.**??**a), energy is provided during the first two jumps, increasing the maximum height attained by the droplet; however, during the third bounce, energy is lost and the initial conditions are recovered. At $\Gamma = 1.82$, the motion is chaotic, and a strange attractor emerges on the Poincaré section (Fig.**??**b). See EPAPS Document No.[ ] for a Smale map diagnostic.

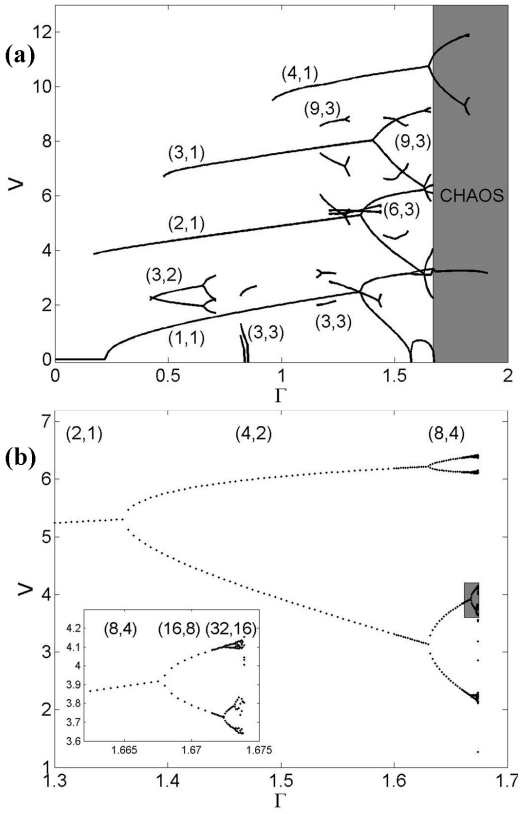

FIG. 6: (a) Bifurcation diagram for $\omega = 1.1$: impact speed V as a function of the forcing acceleration Γ. Note that a mode (m, n) necessarily has n branches. Chaotic solutions first appear at $\Gamma = 1.67$. (b) Period-doubling cascade of the $(2, 1)$ branch. The shaded region is expanded in the inset.

A bifurcation diagram (Fig.**??**a) represents the solution of Eq.(**??**) as a function of Γ for $\omega = 1.1$. For $\Gamma < 0.17$, no periodic bouncing states are possible: the droplet resides at rest on the soap film. The first periodic solution $(2, 1)$ appears at $\Gamma = 0.17$. As Γ is progressively increased, simple modes $(m, 1)$ and complex modes (m, n) appear in turn. At branch points, modes (m, n) execute a period doubling transition to a $(2m, 2n)$ mode. For example, the mode $(2, 1)$ gives rise to a period doubling cascade that terminates at $\Gamma \simeq 1.67$ (Fig.**??**b). Thereafter, the complex periodic modes degenerate into

a strange attractor that may coexist with stable periodic orbits emerging from other branches (shaded area in Fig.??a). For $\Gamma > 1.91$, no such periodic branches persist and the chaotic attractor is the only attracting set.

During the period doubling cascade of $(2,1)$, bifurcations occur at $\Gamma = 1.361$, 1.631, 1.6679, 1.67244, 1.67319, 1.673349, 1.673380,.... Defining $\delta_i = (\Gamma_{i+1} - \Gamma_i)/(\Gamma_{i+2} - \Gamma_{i+1})$ yields the first terms of the δ suite as 7.3, 8.1, 6.0, 4.7, 5.1, ... This suite slowly converges to a value larger than the Feigenbaum constant 4.6692, that is universal for 1-dimension quadratic iterative maps [**?**]. We recall that for area-preserving two-dimension maps, Tabor [**?**] deduces a universal constant of 8.7211. Our two-dimensional non-area-preserving map evidently leads to a suite δ_i that converges to a value lying between those two bounds.

In the bouncing regime, the soap film behaves as a linear spring. The contact time is constant, independent of the impact speed V, and the energy dissipated during impact increases as V^3. These observations guided us in developing a simple model of the bouncing droplet that is in good agreement with experimental results, providing quantitative agreement with the lower order periodic modes, and qualitative agreement with more complex modes. Our system shares many features with the elastic ball bouncing on a vertically vibrated rigid substrate [**?**], including multiperiodicity and period-doubling transitions to chaos. However, qualitative differences exist between the two systems owing to the differences in the collisional dynamics. In the bouncing ball problem, the collision is instantaneous and characterized entirely by the coefficient of restitution; in our system, the collision is of finite duration and the coefficient of restitution depends on the impact speed. Consequently, in our system there are no sticking solutions as arise at weak forcing for the bouncing ball, and the multiperiodicity is considerably enhanced. It is hoped that our study will inform studies of droplets bouncing on a fluid bath [**? ? ? ? ?**]. For example, for droplet bouncing on a soap film, the most unstable bouncing state may be $(2,1)$ rather than the $(1,1)$ observed for the bouncing elastic ball. Finally, we note that in terms of ease of both experimental study and theoretical description, this system is perhaps the simplest fluid chaotic oscillator yet explored.

Acknowledgments

T.G. thanks FRIA/FNRS and Belgian Government for financial support. We gratefully acknowledge Aslan Kasimov, Jeff Aristoff, Pedro Reis, L.Courbin, J-C.Nave, Sunny Jung and Matt Hancock for fruitful discussions.

[] Y. Couder, E. Fort, C. H. Gautier, and A. Boudaoud, Phys. Rev. Lett. **94**, 177801 (2005).
[] S. Protière, A. Boudaoud, and Y. Couder, J. Fluid Mech. **554**, 85 (2006).
[] Y. Couder and E. Fort, Phys. Rev. Lett. **97**, 154101 (2006).
[] S.I. Lieber, M.C. Hendershott, A. Pattanaporkratana, and J.E. Maclennan, Phys. Rev. E **75**, 056308 (2007).
[] T. Gilet and J. Bush, Accepted for publication in J. Fluid Mech. (2008).
[] A. LeGoff, L. Courbin, H. Stone, and D. Quéré, submitted to Europhys. Lett. (2008).
[] D. Richard, C. Clanet, and D. Quéré, Nature **417**, 811 (2002).
[] M. Feigenbaum, J. Stat. Phys. **21**, 669 (1979).
[] M. Tabor, *Chaos and integrability in nonlinear dynamics : an introduction* (New-York, Wiley, 1989).
[] N. Tufillaro, T. Abbott, and J. Reilly, *An experimental approach to nonlinear dynamics and chaos* (Addison Wesley, 1992).
[] T. Gilet, D. Terwagne, N. Vandewalle, and S. Dorbolo, Phys. Rev. Lett. **100**, 167802 (2008).
[] S. Dorbolo, D. Terwagne, N. Vandewalle, and T. Gilet, To appear in New J.Phys. (2008).